

## The dripwaters and speleothems of Poole's Cavern: a review of recent and ongoing research.

Adam HARTLAND<sup>1,\*</sup>, Ian J FAIRCHILD<sup>1</sup>, Jamie R LEAD<sup>1</sup>, David DOMINGUEZ-VILLAR<sup>1</sup>,  
Andy BAKER<sup>2</sup>, John GUNN<sup>1</sup>, Mohammed BAALOUSHA<sup>1</sup> and Yon JU-NAM<sup>3</sup>

<sup>1</sup>School of Geography, Earth and Environmental Sciences, College of Life and Environmental Sciences,  
University of Birmingham, Edgbaston, Birmingham, B15 2TT, UK.

<sup>2</sup>Connected Waters Initiative, University of New South Wales, 110 King Street, Manly Vale, NSW2093,  
Australia.

<sup>3</sup>Multidisciplinary Nanotechnology Centre, School of Engineering, Swansea University, Singleton Park,  
Swansea, SA2 8PP, UK.

\*Corresponding author: e-mail: axh397@bham.ac.uk



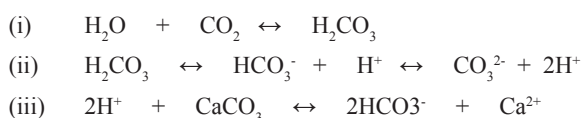
**Abstract:** This paper describes aspects of the geochemical conditions prevalent in the dripwaters of Poole's Cavern, Buxton, UK. We examine what makes Poole's Cavern both highly unusual, and also, extremely useful for understanding geochemical processes, both in hyperalkaline, and natural karstic systems. We review the findings of ongoing research into the colloidal and dissolved organic species and associated trace elements in hyperalkaline dripwaters and show that the composition and appearance of poached-egg stalagmites can largely be explained by the high pH conditions prevalent in their parent waters and the carbon dioxide sources in cave air.

**Keywords:** hyperalkaline; speleothems; organic carbon; trace metals; colloids; CO<sub>2</sub>

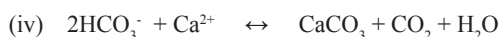
(Received 4 March 2010; Accepted 05 April 2010)

Poole's Cavern (53°12'N 1°56'W), Buxton, UK (mean annual rainfall and temperature 1300mm and 9°C, respectively) occupies an uncommon position among the several types of natural cave systems. If it were not for the legacy of the 19<sup>th</sup> Century lime industry, Poole's would be one of many attractive, but geochemically typical, shallow epigenetic cave systems in the Peak District. However, as a direct consequence of industrial pollution, Poole's is instead a special resource for science: a natural cave system in which the geochemical order has been overturned and a continuum of dripwaters exists, from the normal alkaline (pH 7.5 – 8.5) to the hyperalkaline (pH 9 – 13). The majority of the hyperalkaline percolation waters enter the cavern in the renowned Poached Egg Chamber and precipitate stalagmites at growth rates up to two orders of magnitude greater than is normal for mildly alkaline dripwaters. Natural speleothem extension rates are of the order of tens to hundreds of microns per year (McDermott *et al.*, 1999; Baker *et al.*, 1998); in Poole's Cavern speleothems grow at up to 1cm yr<sup>-1</sup> (Baker *et al.*, 1999), consistent with growth rates (3 – 8mm yr<sup>-1</sup>) for hyperalkaline speleothems reported elsewhere (Sundqvist *et al.*, 2005). Not only is the growth rate of speleothems spectacular, but the mechanism of growth is also quite different from CaCO<sub>3</sub> precipitated at near-neutral pH (MacLeod *et al.*, 1991).

Under normal conditions, rainwater enters soil and dissolves carbon dioxide forming carbonic acid which then dissociates to form bicarbonate ions and protons. The acidity generated then drives dissolution of calcite:



Carbonate dissolution continues until equilibrium is reached. This results in solutions slightly super-saturated with respect to calcite and when the dripwater enters the cave if the partial pressure of carbon dioxide in the solution is greater than that in the cave atmosphere, CO<sub>2</sub> degasses and calcium carbonate precipitates via the reaction:



This describes the geochemical regime at numerous drip points in the cavern. However, underlying the top soil of Grin Low Wood lie laterally varying proportions of lime waste; when rainwater passes

through this waste, calcium oxide is dissolved, producing calcium and hydroxyl ions and resulting in very high pH values (pH 9 – 13):



Above pH 9.5 the normal mechanism of calcite precipitation is overturned (MacLeod *et al.*, 1991) and CO<sub>2</sub> becomes a reagent rather than a product (iv):



These hyperalkaline solutions do not contain enough CO<sub>2</sub> (present as dissolved carbonate ions) to precipitate sufficient calcite to reach equilibrium and instead must sequester CO<sub>2</sub> directly from the surrounding cave atmosphere. Thus, as visitors marvel at the spectacular stalagmites before them, a small proportion of their respired CO<sub>2</sub> contributes to the living rocks that surround them.

The speleothems of Poole's Cavern are also famous for their unusual appearance. In terms of their morphology they typify deposits formed from hyperalkaline solutions and bear close resemblance to stalagmites found in the basements of houses and other buildings in which water has found its way through and dissolved CaO present in the cement used in the mortar (Sundqvist *et al.*, 2005) (Fig.1). The unusual aspect is their colouring – the poached-egg stalagmites are characterized by bright orange tips and to a small extent the hue is also present on their flanks. These stalagmites have generated research interest previously; most notably Baker *et al.* (1999) studied the luminescent properties of stalagmite PC-96-7 and its parent waters. In the dripwater Baker *et al.* (1999) found distinct winter maxima in luminescence intensity indicating higher concentrations of organic (humic-like) compounds and corresponding annual fluorescent laminae in the speleothem. Monitoring of fluorescence intensity in the PC-96-7 dripwater continued for another 3 years and confirmed the seasonal occurrence of winter fluorescence maxima. These previously unpublished data are presented in Fig.2.

Thus, there is substantial evidence supporting the interpretation that the colour of the poached-egg stalagmites originates from organic matter (OM) co-precipitated with calcite during speleothem formation and that higher concentrations of fluorescent OM in wintertime result in annual fluorescent laminations in poached-egg stalagmites. Indeed, anecdotally, staff at the cavern report seeing shifts in the intensity of the orange colour of the tips throughout the hydrological year (A Walker, Cave Manager, *pers. comm.*).

Given that organic fluorescence had already been detected, the high pH dripwaters of Poole's Cavern were identified as suitable for the study of organic matter in cave dripwaters. We were also interested in examining the effects of pH on the reactivity and stability of the organic matter present. Indeed, the stability of organics is vitally important, and this was a major consideration in the selection of Poole's as a study site. We hypothesized that organics in the colloidal size-range (with a dimension between 1nm and 1µm) are more stable in the hyperalkaline dripwaters because of their high pH; at this pH, enhanced deprotonation of functional groups such as phenolic acids, results in increased surface charge of organic colloids (Tipping, 2001), which in turn results in increasing repulsion, decreasing their tendency to agglomerate (Buffle *et al.*, 1998; Lead and Wilkinson, 2006), and hence, enhancing their mobility through the porous matrix.

In the following sections we summarize some of the results of research conducted into the characterisation of organic matter in particulate, colloidal and dissolved phases in Poole's Cavern dripwaters. These findings expand our current understanding of the organic composition of Poole's Caverns speleothems and process controls on the composition and fate of OM in karst groundwaters. In the final section, an extended abstract provides information on ongoing research into carbon dioxide dynamics and hyperalkaline speleothem growth.



**Figure 1a:** Hyperalkaline speleothems formed from waters rich in  $Ca^{2+}$  and  $OH^-$  ions. Poached-egg stalagmites (approx 1m tall) (Photo by I Fairchild). See also figures 1b – 1e.



**Figure 1b:** Re-growth (approx 4cm tall) of poached-egg stalagmite PC-96-7 described in Baker *et al* (1999) the re-growth formed over the period 1997 – 2008 (Photo by A Hartland).



**Figure 1c:** The re-growth sectioned and polished (Photo by A Hartland).

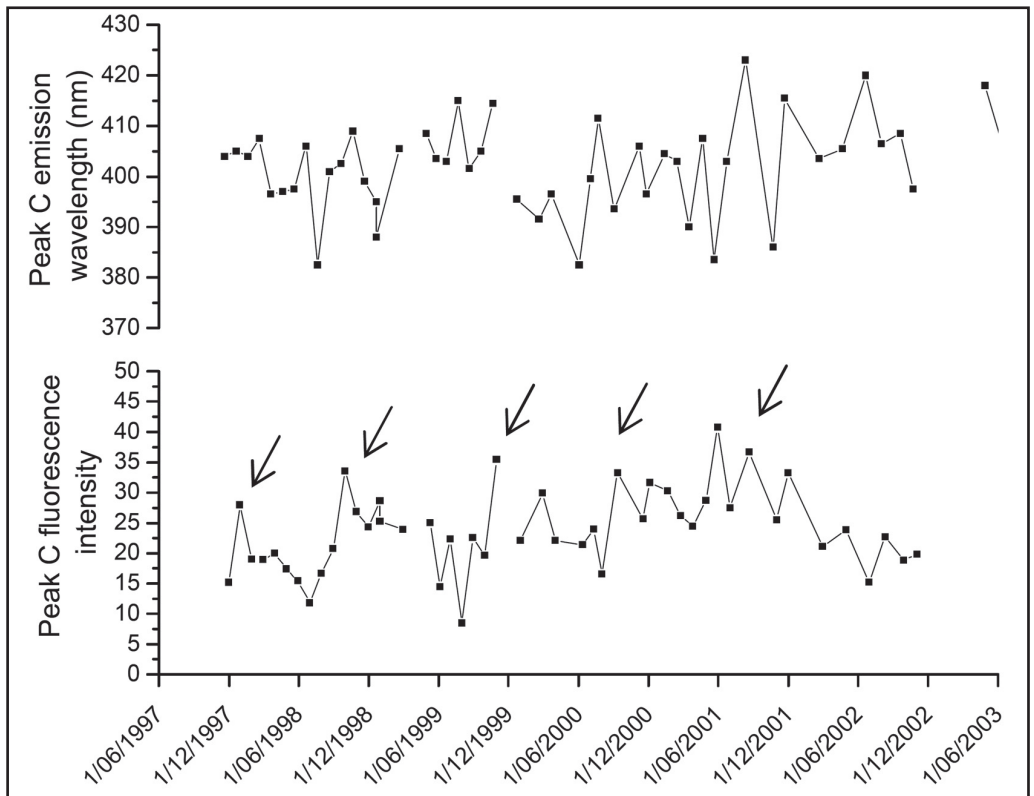


**Figure 1d:** Hyperalkaline speleothems formed in a leaky Texas basement in around 40 years; fingers make Texas Bullhorns sign (Photo by I Fairchild, of a sample retrieved by J Banner).



**Figure 1e:** Array of hyperalkaline speleothems in disused railway tunnel. Note the similar morphology of these speleothems but distinct difference in colour (Photo by J Gunn).

**Figure 2:** Peak C fluorescence intensity and emission wavelength data from the PE1 drip point monitored between winter 1997 and winter 2002 (previously unpublished data). Arrows denote autumn-winter peak in fluorescence intensity. In the autumn-winter of 2002 a breakdown in the seasonal fluorescence signal occurred - possibly due to the digging of drainage channels on the overlying hillside.



### Study site

Poole's Cavern is a shallow epigenetic cave developed in early Carboniferous (Asbian) limestone of the Bee Low Limestone Formation, Peak Limestone Group. Strata exposed within the Cavern are thick, with well-developed cross-bedding, pale-brownish grey, fine- to medium-grained. Volcanic rock horizons intervene locally within the Bee Low Limestone Formation, most notably the Upper Millers Dale Lava Member, at outcrop on the eastern margin of Grin Low, around 750m east of the Cavern entrance. Regionally, the limestone dips in a generally northward direction, inclining between 5 – 10 degrees at the northern edge of the outcrop (Pitty, 1996). Local variations in the angle of dip are exemplified within the Cavern; near the entrance the strata dip northwards at 14 degrees and level out in the main section, becoming essentially horizontal at the inner end of the Show Cave section (Pitty, 1966).

Poole's Cavern is relatively large by comparison to other caves in the Buxton area; it is approximately 240m long and in the largest (main) chamber it is around 15m wide and 20m high. At its base-level the Cavern varies little in altitude, whereas the ground surface above rises continuously at an average of 13 – 15 degrees; hence, the thickness of limestone overburden increases progressively toward the end of the Cavern (Pitty, 1966). The public section of the cave ends at the foot of a boulder slope that can only be penetrated for a few metres at stream level. The boulder choke has also been penetrated at higher level to access two chambers, one of which contains roots from the surface (Gill and Beck, 1991). In Fig.3, a schematic diagram of the Cavern and surrounding buildings is draped over a digital elevation model constructed from LIDAR data (Source: Environment Agency (UK) Geomatics Group) acquired at 1m resolution, which gives an impression of the proximity of the built environment and the topography of the surrounding area.

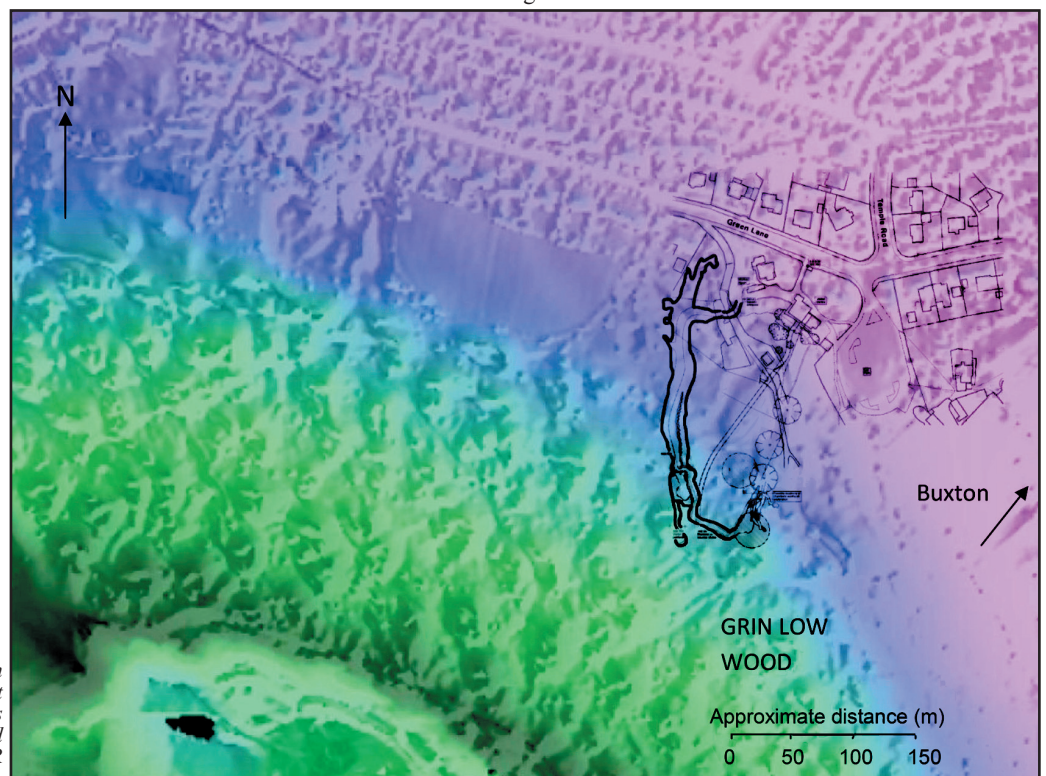


**Figure 3:** The situation of Poole's Cavern with respect to Grin Low and the adjacent urban area. A schematic of the Cavern is overlain on a digital elevation model derived from LIDAR data (1m resolution) (LIDAR data copyright Geomatics Group 2009).

Prior to around 1820, limestone was quarried and burnt on the hillside above the cave; when the industry ceased to be a viable proposition associated lime waste was spread out and trees were planted. In the present day secondary deciduous woodland (Grin Low Wood) is established among the relict lime kilns. Soils consist of leaf litter and organic-rich topsoil (Brown Ranker (Baker and Genty, 1999)) overlying lime waste and fragments of poorly-sorted limestone. As already discussed, the remnants of the lime-burning industry on Grin Low are responsible for the range of geochemical conditions found in Poole's Cavern dripwaters.

The most prominent hydrological feature of Poole's Cavern is an intermittent stream that has been proven by tracing experiments to be fed by sinks on Stanley Moor to the south of the Cavern (Ford and Gunn, 1992). The stream enters the cave from beneath the boulder choke and drains down-dip towards the dry entrance but sinks about 70m before reaching it. The sinking water finally resurges at Wye Head, approximately 500m due north (Ford and Gunn, 1992). In Fig.4, the drip points sampled in recent studies are detailed. Drip points sampled on a monthly basis are highlighted in bold in Table 1. The other drip points were surveyed during sampling trips in October 2008 but were not studied further. Data presented in Table 1, which correspond to those drip points monitored on a monthly basis, are the averages and standard deviations from one year of measurements.

### Materials and methods

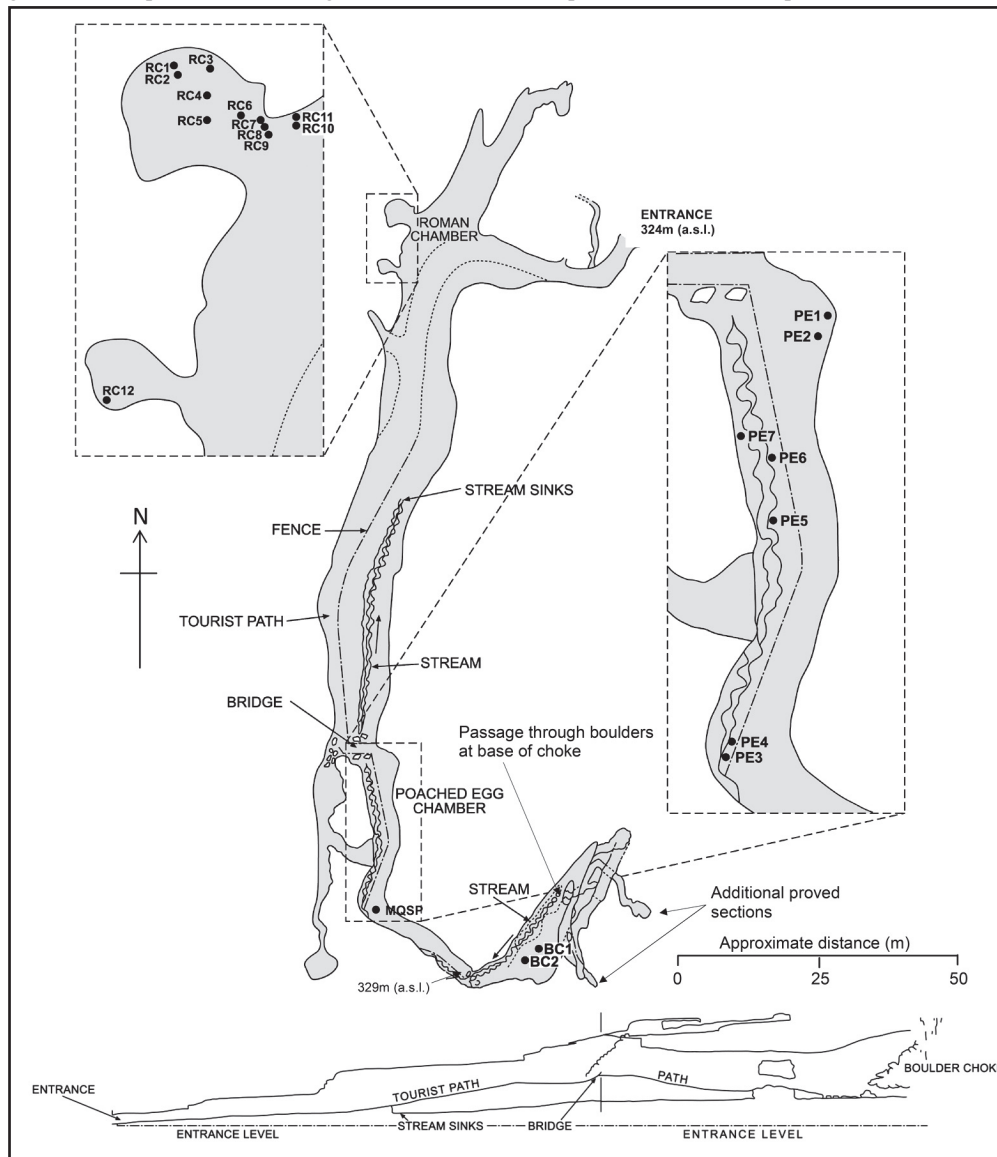
A comprehensive description of the methodologies and instrumental techniques employed in the determination of all the analyses described herein would be too lengthy and of little relevance to the broad readership to which this paper is aimed. Thus, we give only a very general description here, although more information is provided on

the readily accessible techniques. In Fig.5, the multi-methodological approach employed in the sampling and analysis of Poole's Cavern dripwaters is summarized.

Samples were taken using acid-washed (10% HNO<sub>3</sub> followed by thorough soaking in de-ionized water (DIW)) HDPE funnels and 500 ml sample bottles. Samples were typically collected over a period of 24 hours. The conductivity and pH of dripwaters were determined in the field and aliquots were taken for determination of anion and cation concentrations. Raw samples were filtered using membranes with a nominal pore size of 1µm in the field and then filtered and ultrafiltered (pore sizes of 0.1µm and 1 kDa) in the laboratory within 18 hours of collection. Filtration at 0.1µm utilized a Millipore Sterifil™ system attached to an electric air pump. Ultrafiltration at 1 kDa was achieved using an Amicon stirred-cell ultrafiltration system at low-flow (4 bar N<sub>2</sub>). Sub-samples were taken at each point for determination of fluorescence signatures, total organic carbon concentration (TOC) and trace element concentrations. Filters were cleaned extensively prior to use with de-ionized water and 10% HNO<sub>3</sub> in a ratio of 3:1 in order to reduce the organic and trace element blanks from the filters.

### Fluorescence spectroscopy

Fluorescence spectra were obtained using a Varian Cary Eclipse™ fluorescence spectrophotometer equipped with a Peltier temperature controller using a 4ml, 1cm path length cuvette. Samples were analysed using methods previously published by Baker (2001), whereby fluorescence emission-excitation matrices (EEMs) were generated by scanning and recording emission spectra from 300 to 500nm at 0.5nm steps with 5nm increments of excitation wavelength between 280 and 400nm. Excitation and emission slits were set to 5nm and the analytical temperature and PMT voltage were set to 20 ± 0.1°C and 770 V.



Drip point	pH	Electroconductivity (mS cm <sup>-1</sup> )
<b>RC1</b>	<b>12.3 ± 0.6</b>	<b>2.08 ± 1.38</b>
<b>RC2</b>	<b>12.4 ± 0.5</b>	<b>2.26 ± 1.25</b>
RC3	8.1	0.61
RC4	7.9	0.51
RC5	12.3	1.18
RC6	8.4	0.25
RC7	8.2	0.34
RC8	8.2	0.37
RC9	8.1	0.47
RC10	7.7	0.53
RC11	7.7	0.52
RC12	7.6	0.52
RC13	7.9	0.60
<b>PE1</b>	<b>11.7 ± 0.4</b>	<b>0.70 ± 0.24</b>
PE2	11.8	0.76
PE3	11.8	0.60
PE4	11.7	0.76
PE5	11.6	0.66
PE6	12.1	1.34
PE7	11.8	1.00
<b>BC1</b>	<b>7.9 ± 0.2</b>	<b>0.48 ± 0.04</b>
<b>BC2</b>	<b>7.9 ± 0.2</b>	<b>0.49 ± 0.04</b>
MQSP	7.8	0.45

Table 1: Summary pH and electroconductivity data from surveyed and monitored drip points. Reference numbers of drip points monitored for organic colloids are **emboldened**.

Figure 4: Schematic of Poole's Cavern with the locations of sampled drip points indicated. Drip points sampled for colloidal materials are shown **emboldened** in Table 1.

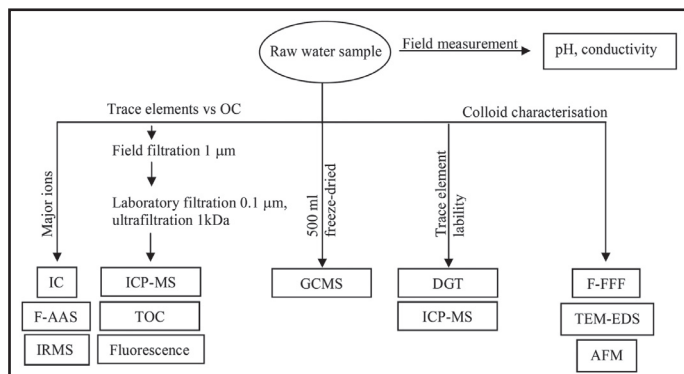


**Figure 5:** Multi-methodological approach adopted for the analysis of cave dripwater. ICP-MS = Inductively Coupled Plasma Mass Spectrometry; TOC = Total Organic Carbon; DGT = Diffuse Gradients in Thin Films; IC = Ion Chromatography; F-AAS = Flame Atomic Absorption Spectrometry; IRMS = Isotope Ratio Mass Spectrometry; GCMS = Gas Chromatograph Mass Spectrometry; F-FFF = Flow Field-Flow Fractionation; TEM-EDS = Transmission Electron Microscopy-Energy Dispersive Spectrometry; AFM = Atomic Force Microscopy.

Calibration of the spectrophotometer was performed via measurement of the Raman intensity at 395nm emission using a sealed distilled water cell. Raman intensity was measured approximately every 15 analyses and averaged  $26.7 \pm 0.76$  over the period August 2008 to August 2009. All fluorescence intensity values reported in this manuscript are corrected using the Raman peak intensity (no instrument-specific correction was performed). Results from procedural blanks demonstrated that organic carbon leached from filter membranes was non-fluorescent and blank values were equivalent to de-ionized water.

### Total organic carbon

TOC concentration was determined using a Shimadzu TOC-V, high-temperature combustion analyser following the non-purgable organic carbon (NPOC) method. Samples were acidified with ultrapure hydrochloric acid to produce carbon dioxide, which is measured by infrared detection, and then subtracted from TOC, which was determined by oxidation of organic carbon by high-temperature combustion. Each reported measurement is the average of 4 – 10 injections, with standard deviations reported as an estimate of error. De-ionized water blanks produced following the same procedure used in sample collection and preparation averaged  $0.1 \pm 0.1 \text{ mg l}^{-1}$ . Instrumental drift and changes in analytical accuracy were addressed by the integration of check standards into the calibration on each run.  $R^2$  values for calibration curves were typically better than 0.98. TOC concentrations in sequentially filtered samples were quantified following procedural blank correction.

### Microscopy

Samples for atomic force microscopy (AFM) were prepared using the adsorption method, whereby a freshly-cleaved  $1 \text{ cm}^2$  mica sheet was immersed in the sample for 30 minutes. The sheet was then removed and rinsed with de-ionized water and dried under ambient conditions in a covered Petri dish to prevent airborne contamination. All AFM images were obtained using an XE-100 AFM (Park systems). The measurements were carried out in the non-contact mode using Si cantilever with a spring constant of  $42 (10 \sim 130) \text{ N m}^{-1}$  (Nanosensors, 910 (U)-NCHR). All scans were carried out in air, at room temperature. Images were acquired in true non-contact mode and recorded in topography mode with a pixel size resolution of  $256 \times 256$  and a scan rate of  $0.5 - 1.0 \text{ Hz}$ . Height measurements of adsorbed ultra-fine (nano) colloids were made using the section analysis software of the microscope. TEM samples were prepared onto copper TEM grids (Agar Scientific) using the direct ultracentrifugation at  $150000g$  on a Beckman ultracentrifuge (L7-65 Ultracentrifuge) with a swing out rotor SW40Ti (Wilkinson *et al.*, 1999) within 24 hours of sample collection in order to retain the true aspect of the native colloidal pool (Mavrocordatos *et al.*, 2000). Samples were analysed within 2 weeks of preparation using a TECNAIF20 Field Emission gun transmission electron microscope coupled with an x-ray Energy Dispersive Spectrometer (X-EDS) from Oxford Instruments.

### Results and discussion

#### Fluorescence characteristics of organic carbon in dripwaters

The fluorescent characteristics of OM sampled from Poole's Cavern dripwaters were determined using 3D Emission Excitation Matrices (EEMs), essentially, maps of fluorescence intensity in optical space. Fluorescence occurs when electrons that have been excited to a higher energy state (by a light source) return to their ground state and release energy in the form of light (Lakowicz, 2006). Emission of fluorescence occurs at a longer wavelength than the wavelength of excitation and emission predominantly occurs in longer wavelength UV and blue wavelengths (300 – 500nm) corresponding to excitation by UV light between 200 – 400nm. Fluorescence in natural waters is typically generated by organic (humic-like and fulvic-like) compounds and amino acids (or proteins containing tryptophan) (Baker *et al.*, 2008).

In Poole's Cavern, fluorescence signatures were detected in wavelength regions associated with humic- and fulvic-like compounds; specifically, fluorescence at the excitation-emission pair of 290–340:395–430nm (peak C) and the excitation-emission pair of 265–280:300–370 (peak A). In Fig.6, examples are given of typical fluorescence signatures of OM in high pH and normal pH dripwaters (the peak A and C fluorophores are indicated on the top left plot). Close attention should be paid to the scales used in each plot: fluorescence

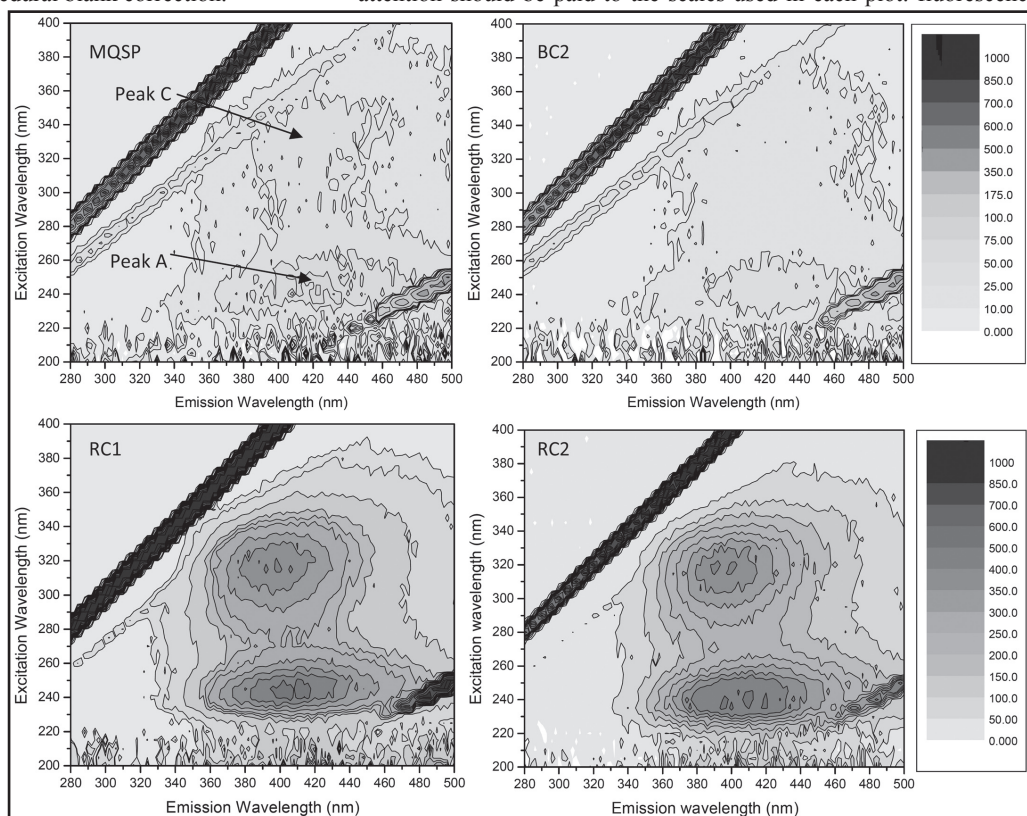


**Figure 6:** Representative fluorescence excitation-emission matrices (EEMs) from normal (pH 7.5–8.1) and hyperalkaline (pH 9.5–13) dripwaters.

intensities of OM sampled from the high pH (pH > 12) dripwater were around an order of magnitude higher than those detected in the pH 7.5 – 8.5 water samples. The high pH dripwaters were found to fluoresce at consistently shorter wavelengths than those compounds sampled in lower pH drips. Following pH-adjustment experiments it was found that the shorter wavelengths of emission exhibited by these compounds were pH-sensitive and at lower pH values peak C emission trended towards longer wavelengths. The intensity of fluorescence was also found to increase strongly (up to 100%) in a pH range of 7 – 12 (Hartland *et al.*, in prep.).

Spectral shifts and increases in fluorescence intensity at high pH values have been reported before (e.g. Patel-Sorrentino *et al.*, 2002; Spencer *et al.*, 2007). However, the extent of the pH-sensitivity of OM in the hyperalkaline drips was found to be unusually high: around an order of magnitude greater than is typically found (Tam and Sposito, 1993; Mobed *et al.*, 1996; Patel-Sorrentino *et al.*, 2002; Spencer *et al.*, 2007). Increases in fluorescence intensity at high pH reflect changes in the coordination environment of fluorophores. For example, deprotonation of functional groups may result in an increase in intra-molecular repulsion, causing the compounds to attain extended configurations (Tipping, 2001), thus increasing the exposure of fluorescent moieties to the light source. This may be indicative of the presence of more humic-like OM in the hyperalkaline dripwaters than is typically found under near-neutral pH conditions in cave waters. Alternatively, this high degree of pH sensitivity might be the result of substantial chemical changes such as oxidation of the OM under the high pH conditions.

### Total organic carbon in waters and speleothems

The TOC concentration in sequentially-filtered dripwater samples was determined following a blank correction procedure. However, because the organic carbon blank was cumulative, the limit of detection (3 x standard deviation of the blank) increased with each successive filtration step. Thus, the available data in the smallest size fraction (< 1 kDa) are limited. Also, in the normal (near-neutral) pH dripwaters sampled the TOC concentration in the raw (unfiltered samples) was found to be around half that in the high pH dripwaters and so determination of TOC below 1nm was, in effect, not possible.

Results from OC determinations demonstrate that the concentration of organic carbon in the colloidal size range was substantially greater in the hyperalkaline dripwaters (Fig.7). Over a year of monthly observations, the mean concentration of OC in hyperalkaline dripwaters with a dimension between 1µm and 1nm was 2.7mg l<sup>-1</sup>; whereas, the mean concentration of OC in the pH 7.5 – 8.1 dripwaters in the same size range was 0.3mg l<sup>-1</sup> (Hartland *et al.*, in prep.). This is evidence of charge-stabilisation of colloidal OM at high pH and hence, for the lower stability of colloidal OM in karst dripwaters at near neutral pH values. This argument is based on the sequential nature of the soil-aquifer system, whereby infiltrating waters mobilize organic colloids from the soils (which from surveys of the soils at the site have been confirmed to overlie the lime waste at the investigated locations) and then subsequently attain high pH values following dissolution of CaO; i.e. the inputs of colloidal OM into groundwater are essentially uniform. All else being equal, we can reasonably suppose that in the normal range of pH, agglomeration and deposition driven by relatively high Ca concentrations and long residence times are important process controls on the mobility of colloidal OM in karstic aquifers.

Calcium (II) is an effective coagulant, which causes destabilisation of colloids through compression of the electric double layer of electrolytes that surround colloids and screen their interactions (Buffle *et al.*, 1998). As predicted by DLVO (Derjaguin and Landau, Verwey and Overbeek) theory, at higher ionic strength the double layer is compressed allowing colloids to come into closer proximity and at very close range, attractive London-van der Waals forces can exceed repulsion (Buffle *et al.*, 1998). Thus, when the net force is one of attraction, aggregation occurs and when aggregates become sufficiently large (i.e. > 1µm) deposition under gravity may occur.

Given the much higher organic carbon content of the hyperalkaline dripwaters it is reasonable to speculate that the colour of the poached-egg stalagmites reflects their higher organic contents. Indeed, analyses of the TOC contents of the PE1 speleothem (re-growth of PC-96-7) indicate that the organic content of Poole's Cavern's poached-egg stalagmites is greater than other hyperalkaline precipitates collected in the Roman Chamber (which are less strongly coloured). The mean TOC content of stalagmite PE1 was found to be 0.80 ± 0.34mg g<sup>-1</sup>

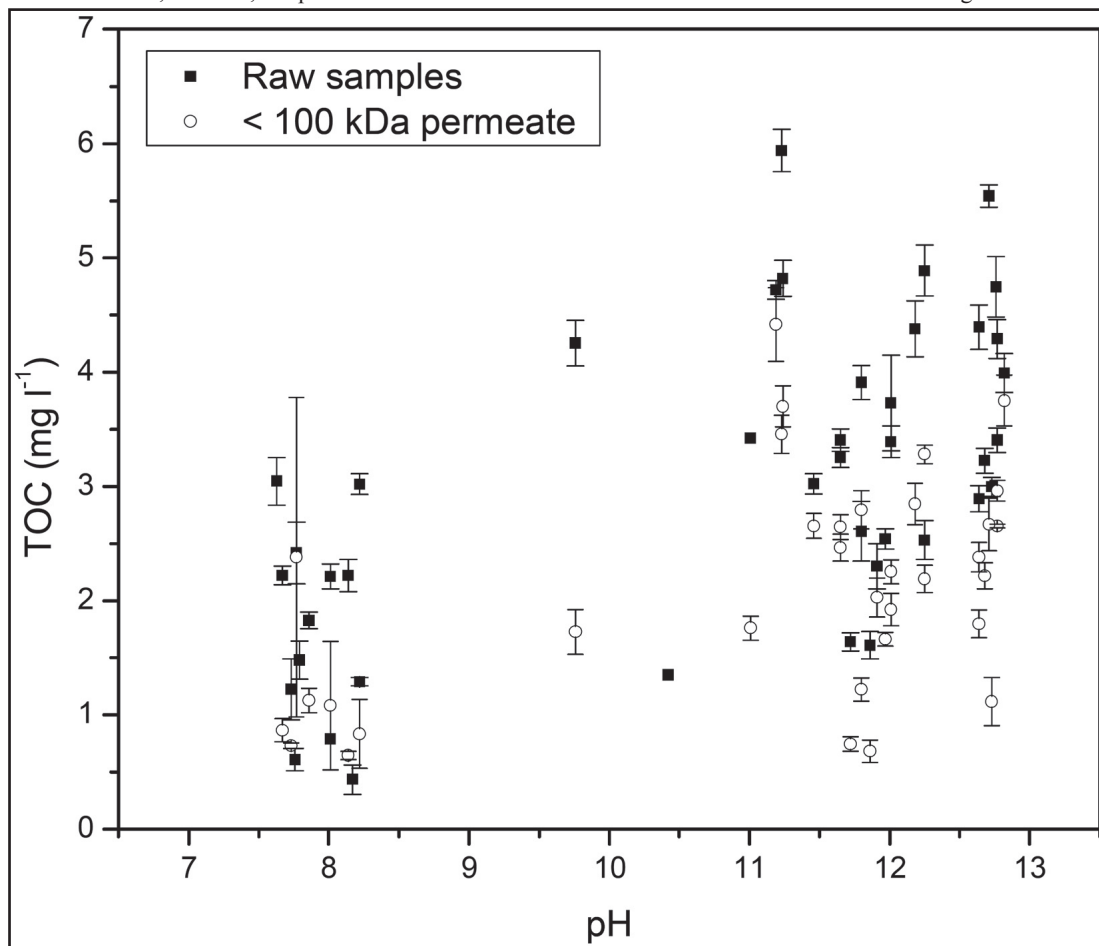


**Figure 7:** The relationship between TOC concentration and pH in raw samples and those filtered at 100 kDa (nominal pore size 0.1µm). Higher concentrations of colloidal and particulate OM in high-pH dripwaters are attributed to charge stabilization. Data points are the mean values of between three and eight replicated analyses. Error bars are the standard deviations of the replicated analyses. Measurements of pH are accurate to ± 0.1 units.

calcite whereas the mean TOC concentration in precipitates formed under drip points RC1 and RC2 were  $0.45 \pm 0.02$  and  $0.12 \pm 0.01 \text{ mg g}^{-1}$ , respectively (TOC contents were determined following dissolution of calcite powders in 2M Ultrapure HCl and dilution with de-ionized water).

This variation in the OC contents of the hyperalkaline precipitates studied is somewhat surprising given that the mean organic carbon concentrations in the three dripwaters were similar ( $4 \pm 0.4 \text{ mg l}^{-1}$ ). In addition, fluorescence analyses of OC in the three dripwaters revealed little difference in their intrinsic fluorescent attributes (Hartland *et al.*, in prep.). Hence, compositional factors such as the degree of hydrophobicity/hydrophilicity of OC in the dripwater may reasonably be discounted. We speculate therefore that the higher OC content of the PE1 speleothem might be related to its growth rate.

In addition, OC concentration in powders drilled from alternating pale and dark (fluorescent) laminae in the PE1 speleothem were determined. However, no clear association between OC concentration and laminae colour in the PE1 sample was found. In some years OC concentrations were higher in fluorescent laminae (2000 – 2001) and in other years concentrations were higher in the paler (non-fluorescent) laminae (2005 – 2007). As discussed later, the growth rates of the hyperalkaline speleothems are thought to vary dynamically seasonally, with generally greater growth rates in the summer. Therefore, given the apparent lack of OC structure between seasons, it might be that OC incorporation in the hyperalkaline speleothems is constrained by variations in growth rate at the time of formation, or variations in OM composition - not detected from monitoring of fluorescence attributes. No quantitative data are currently available on the extension rates of hyperalkaline speleothems in the Roman Chamber, but the  $\text{pCO}_2$  of air in Roman Chamber is likely to be lower than that in the Poached Egg Chamber; as will be discussed below, because  $\text{CO}_2$  is a reactant in calcite precipitation above pH 9.5, this might limit the extension rates of hyperalkaline speleothems in the Roman Chamber to a greater extent than in the Poached Egg Chamber.

Returning to consideration of the unusual appearance of poached-egg stalagmites, we recall that the nature of the fluorescent fraction of OM in hyperalkaline drips is quite distinct from that of normal aquatic OM and therefore, that the highly coloured appearance of the stalagmite

growth tips might not only reflect higher organic carbon content of the speleothems. One other notable quality of these speleothems is that the ones *in situ* are indeed very brightly coloured, but those that have been removed (and exposed to daylight) have lost their orange hue over time (as evidenced by the specimens displayed in the Poole's Cavern Museum). Hence, the organic matter present in the speleothems is also apparently affected by photodegradation. If this is the case then it is another compelling reason to limit the exposure of the speleothems to light and should perhaps be factored into cave management decision-making.

### Trace element binding by organic colloids

A major focus of the recent research conducted at Poole's has been on the extent to which higher pH values affect the binding of trace metals in solution by organic colloids and dissolved organic compounds. This process was brought to the attention of the cave science community in a paper by Borsato *et al.* (2007) who demonstrated an association between organic-bearing fluorescent laminae in speleothems from Grotta d'Ernesto in northeastern Italy, and increases in the abundance of trace elements known to coordinate preferentially with oxygen-containing groups in organic ligands by reactions of the form in equation (viii). The apparent trace element hierarchy was  $\text{Y} > \text{Zn}, \text{Cu}$  and  $\text{Pb} > \text{P}$  and  $\text{Br}$ , where P and Br are considered to be structural components of the organic matter (Borsato *et al.*, 2007). If these elements can be shown to have a specific association with OM in cave dripwaters then it might be possible to make a direct link (conceptually, and perhaps quantitatively) between their abundance in speleothems and colloidal migration in groundwaters (Fairchild and Hartland, 2010).



... where  $\equiv\text{S}$  represents the structural cation(s) to which a surface O atom is attached. The functional group valency is omitted for convenience.

The relationship between OC concentration (ppm), pH and Cu, Ni, Co and Sr concentration (ppb) is shown in Fig.8. Elements that do not coordinate strongly (inner-spherically) with organic ligands are not expected exhibit positive changes in their ratio with organic carbon with increasing pH. For example, the alkaline earth metals (Sr, Ba, Mg) are thought only to coordinate with functional groups in OM via non-specific formation of ion pairs (Bradl, 2004) although most of

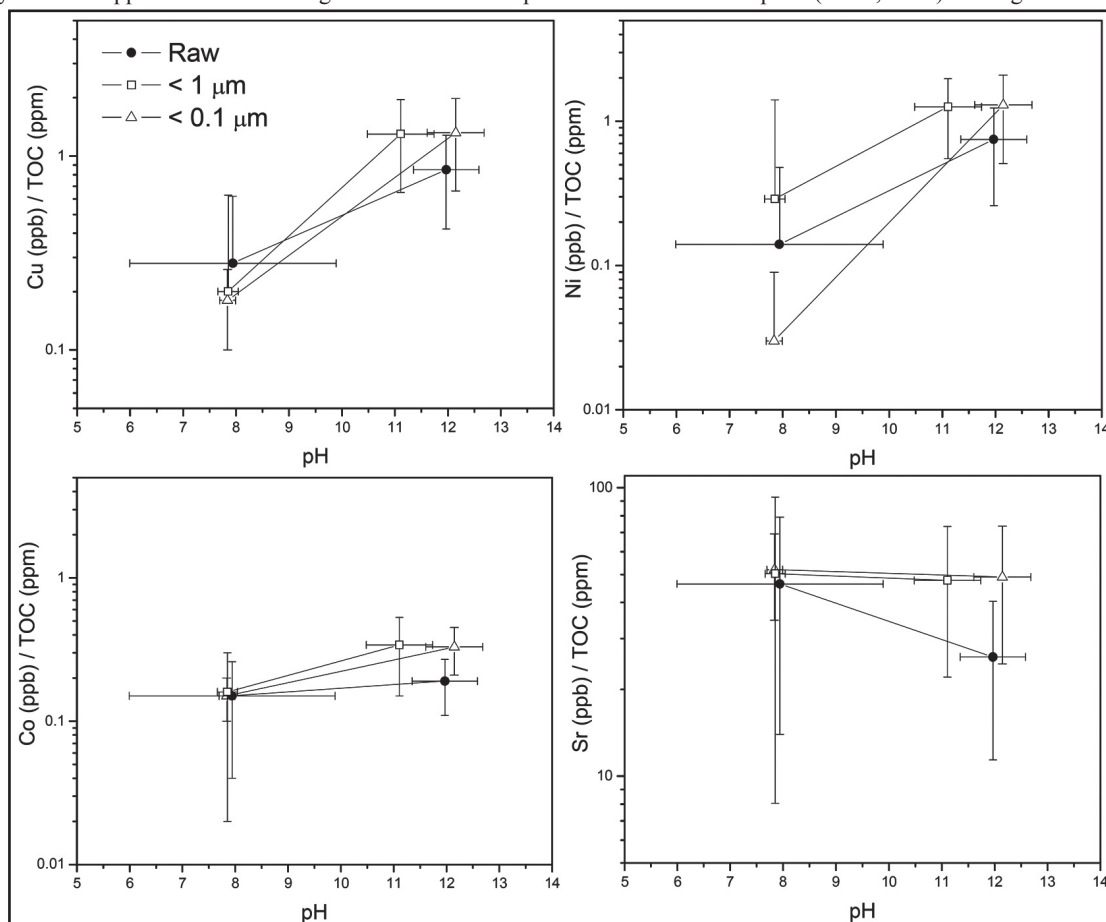


**Figure 8:** Ratios of Cu, Ni, Co and Sr (ppb) to TOC (ppm) in size-fractionated Poole's Cavern dripwater samples plotted as a function of solution pH; values are averages and error bars represent the standard deviations of measurements conducted over a year of monthly sampling. Cu and Ni ions show elevated binding affinity ( $> \text{Co}$ ) for NOM at higher pH values in line with predictions; Sr / TOC ratios are indifferent to pH change as expected for alkaline earth metals. Lines connecting data points are intended to aid in interpretation and do not reflect the ratios of trace metal:TOC at intermediate pH values.

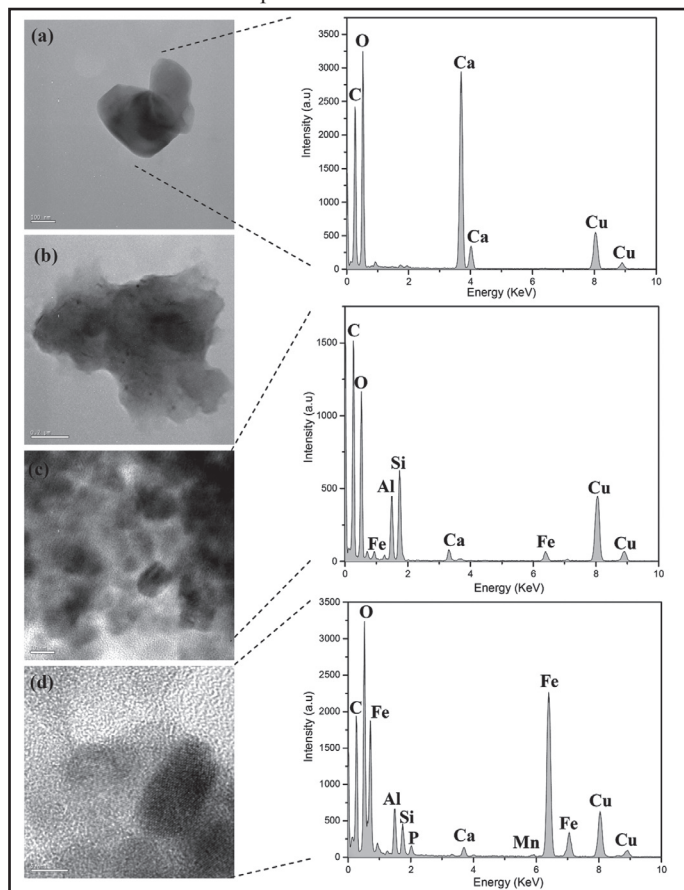
the available data relate to clay colloids (Chen and Hayes, 1999; Zhang *et al.*, 2001). When the number of reactive sites in organic ligands and colloids increases (due to deprotonation at high pH) these elements are out-competed by elements that show a greater specificity (e.g. Cu, Ni and Co) (Bradl, 2004). Results from analysis of TOC and trace element concentrations in Poole's Cavern dripwaters appear to confirm this prediction: the alkaline earth metal Sr does not show a positive shift in its ratio with TOC at elevated pH values (Fig.8) whereas, the ratios of Cu and Ni > Co are elevated at high pH in line with reported data on the binding affinity of these metals for oxygen-containing functional groups of organic ligands (Bradl, 2004).

As reported in Fairchild and Hartland (2010), both V and Cr are also well-correlated with TOC concentration at increasing pH in Poole's Cavern samples. However, in investigations of the trace metal contents of sequentially-filtered dripwaters both Cr and V were only slightly reduced in concentration by ultrafiltration at 1 kDa, whereas, Cu, Ni and Co were generally reduced in concentration by around 40 – 50% (Fairchild and Hartland, 2010). Therefore, the bulk of the Cr and V in solution must have been present in the truly dissolved phase. The trace element binding behaviour of organic matter in Poole's Cavern dripwaters is an ongoing area of research. In particular, we aim to determine whether Cr and V are bound by dissolved organic solutes and whether variations in abundance of colloid-associated elements in dripwaters during hydrologically active periods are reflected similarly in speleothems.

### Morphology and qualitative chemical composition of colloidal materials

Transmission electron microscopy (TEM) coupled to an x-ray Energy Dispersive Spectrometer (X-EDS) was used to obtain information on the morphology and qualitative chemical composition of colloids in both high pH and normal pH dripwaters. Some reconnaissance Atomic Force Microscopy was also employed to examine the particle height distribution of colloids.

Representative TEM images and EDS spectra are given in Figs 9 and 10. Numbers of coarse colloids and aggregates (100nm to > 1µm) in the near-neutral (pH ≈ 8) and hyperalkaline (pH ≈ 12) dripwaters were comparable, whereas smaller colloids < 100nm were generally much less numerous and overall the numbers of particles imaged were not sufficient to construct particle size distributions.



The morphology of colloids in the BC1 and RC2 samples was typical of that reported previously (Fairchild and Hartland, 2010), being principally amorphous aggregates of what is presumed to be organic matter with aluminosilicates and iron oxides, which based on their elemental composition were the predominant classes of inorganic colloids found. Calcite colloids were found in all dripwater samples investigated, although these were the least numerous of the colloid classes detected. EDS spectra indicate small amounts of Mn and Ti are present in some particles. Concentrations of Fe, Ti and Mn in Poole's Cavern dripwaters were generally low, and were detected inconsistently during temporal monitoring of trace elements in dripwaters; transient increases in the concentration of Ti, Fe and Mn might possibly reflect ephemeral pulses of oxide-rich colloids and aluminosilicates (Ti expected to be a structural component of the latter) and there is some evidence from speleothems in other cave systems to suggest that Mn and Fe colloids may be more abundant in dripwaters during hydrologically active periods (Richter *et al.*, 2004). Also, the concentrations of Ti, Mn and Fe showed no apparent association with total organic carbon and did not increase in their ratio with TOC at elevated pH.

In the samples studied by TEM, clear evidence for aggregation of fine colloids was found (Fig.10a). Images 9 (c) and (d), and 10 (a) and (b) appear to show aggregates composed of large numbers of < 10 nm-sized spherical colloids and darker zones shown to be regions rich in iron oxides in the magnified images. Colloid composition in Poole's Cavern dripwaters thus appears to be fairly consistent between the drips studied, with the extent of aggregation being possibly determined largely by the prevailing hydrogeochemical conditions. The PE1 dripwater is unique amongst the dripwaters studied in that the ionic strength is comparable to more typical karstic dripwaters (e.g. BC1 and BC2, EC ≈ 500), but the pH conditions are consistently high (i.e. between pH 11 and 12). It is hypothesized therefore that this combination of high pH and moderate ionic strength may result in enhanced stability of organic colloids in the nanoparticulate size range in PE1 dripwater, whereas, in the BC1 and RC2 dripwater, colloids may aggregate more readily. Preliminary evidence from AFM imaging of the ultra-fine (nano) colloidal fraction appears to support this hypothesis (Fig.11). In Fig.11, particle height measurements of natural aquatic colloids adsorbed on a mica sheet are given. In conjunction with the evidence from TEM analyses, this indicates that natural colloidal entities are present in a continuum in

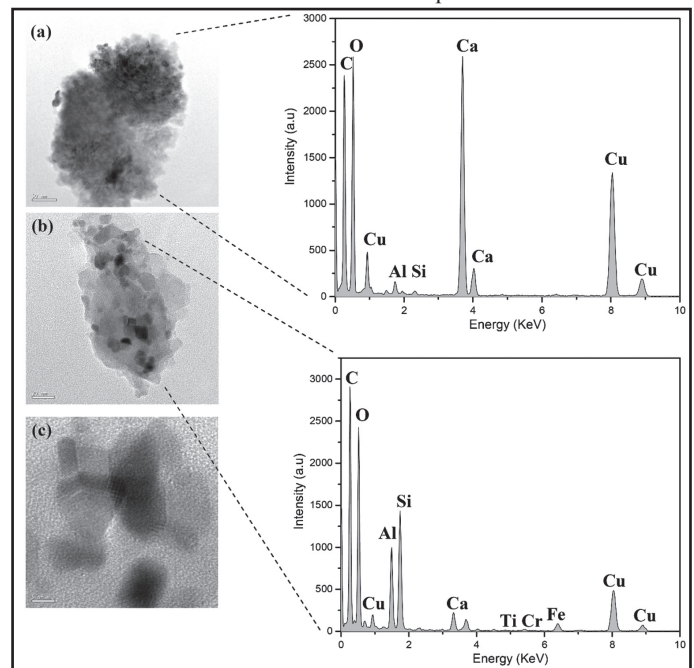
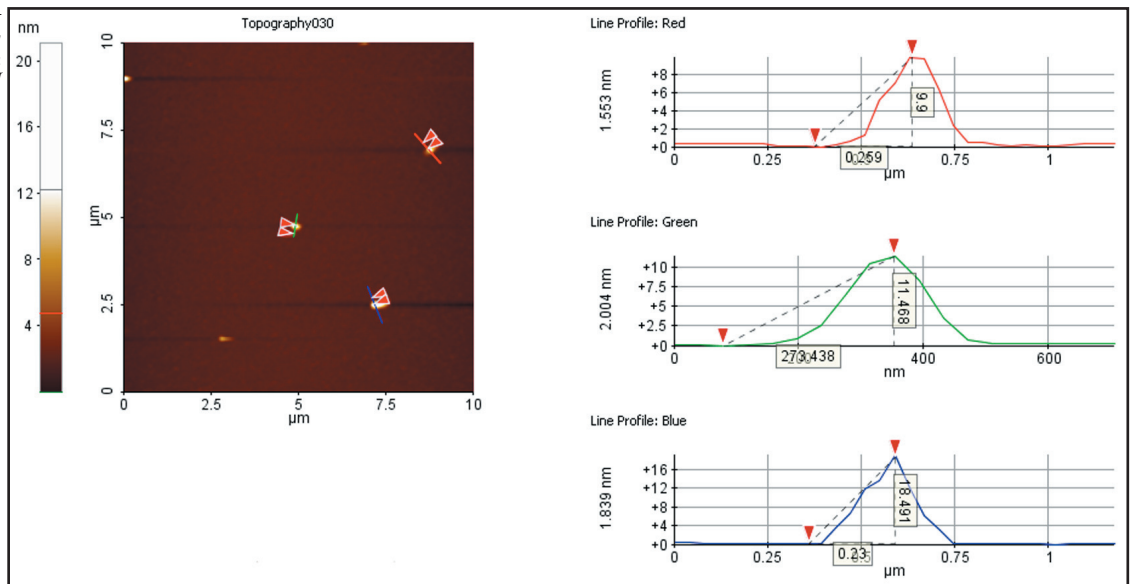


**Figure 10:** Representative TEM images and X-EDS spectra from RC2 dripwater sampled in June 2009, (a) aggregate of fine organic colloids, iron oxides and  $\text{CaCO}_3$ , (b) aggregate of aluminosilicates, organic matter and iron oxides, (c) magnification of (b) showing iron oxide colloids, parallel lines are diffraction from atomic planes. Cu and C peaks in spectra originate from supporting grid.

**Figure 9:** Representative TEM images and X-EDS spectra from BC1 dripwater sampled in June 2009, (a)  $\text{CaCO}_3$ , (b) aggregate of organic matter, aluminosilicates and iron oxides, (c and d) magnification of section of (b) showing iron oxide colloids, parallel lines are diffraction from atomic planes. Cu and C peaks in spectra originate from supporting grid.



**Figure 11:** AFM Image including particle height data. AFM results show that colloids are present with dimensions <10nm in high pH dripwater samples.



karstic dripwaters from the nanoparticulate (1 – 100nm) through to the coarse colloidal (100nm – 1μm) and particulate (> 1 μm). Further research is needed to assess the relative importance of these colloidal classes in terms of hydrogeochemical processes in speleothem-forming dripwaters (e.g. colloid-facilitated transport of trace metals). This discussion of the processes governing colloid size in cave dripwaters is speculative but, nevertheless, these are the most detailed data available to date on the composition and morphology of natural colloids in cave dripwaters.

### Carbon dioxide dynamics and stalagmite growth

In this section, we present an extended abstract of ongoing work related to the petrology of the stalagmites and the role of cave air in their formation. Stalagmites forming from waters of normal pH typically grow upwards at 0.01 – 1mm yr<sup>-1</sup>. These growth rates tend to increase with environmental temperature, because soil pCO<sub>2</sub> increases at higher temperature in-line with increases in microbial biomass. Where cave pCO<sub>2</sub> is seasonally high (typically in summer), CO<sub>2</sub> degassing, and thus growth are inhibited. In the low-pCO<sub>2</sub> season (usually winter), CO<sub>2</sub>-degassing from dripwaters (and thus growth rate) is enhanced. Growth of stalagmites may also be limited by the quantity of dripping water where this is small. In contrast, hyperalkaline waters tend to produce stalagmites that grow at rates of 1 – 10mm yr<sup>-1</sup> as shown at Poole's by Baker *et al.* (1999).

A stalagmite sampled in the Poached Egg Chamber in 1996 from drip PE1 was described by Baker *et al.* (1999). New growth has occurred at this site in the intervening period at a mean rate of 4mm yr<sup>-1</sup> (Fig.1). We have compared the mass accretion (around 3.6 g yr<sup>-1</sup>) with the supply of Ca, using the Ca content and drip rate and find that only around 20% of the Ca supplied has been precipitated in the stalagmite. This implies, from equation (vi), that the supply of CO<sub>2</sub> limits stalagmite growth as discussed by Clark *et al.* (1992). Accordingly we have investigated the dynamics of air circulation and CO<sub>2</sub> supply in the cave.

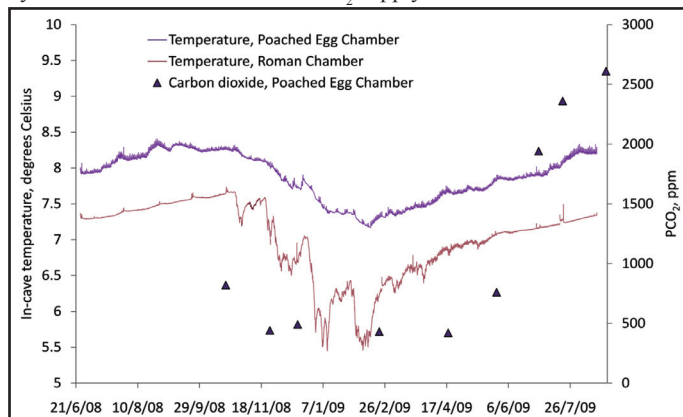


**Figure 12:** Seasonal variations in temperature and pCO<sub>2</sub> in Poached Egg Chamber and Roman Chamber (temperature only) during the period June 2008 to July 2009. The carbon dioxide measurements represent minimal values, i.e. without additional CO<sub>2</sub> from cave visitors.

Observations in 2008–2009 have verified and extended the conclusions of Smithson (1991) who showed that when the external temperature dropped below around 7°C, external air penetration into the Roman Chamber was enhanced, but that a more stable situation applies to the upper, interior part of the cave (Fig.12). In Poached Egg Chamber, temperature shows a small annual range of about 1°C, about half that of Roman Chamber where winter temperatures are in-phase with fluctuations in the exterior, but much damped. In Poached Egg Chamber, from November to April, CO<sub>2</sub> concentration is 400 – 500 ppm, not much higher than the external atmosphere (380 ppm), but it rises to over 2500 ppm in August (Fig.12). Using the approach of Faimon *et al.* (2006), we have made use of the disturbance to CO<sub>2</sub> levels caused by the presence of cave visitors to analyze the system.

On about half the periods monitored, CO<sub>2</sub> did not display clear diurnal cycles related to the addition and decay of an anthropogenic CO<sub>2</sub> signal – this is probably related to meteorological factors influencing air circulation, but no common pattern was found. Also spot measurements of carbon dioxide and radon outside the monitoring periods indicate a higher level of variability and more detailed monitoring is required to determine the nature and causes of this variation. However, on the other half of the monitoring periods, a fairly regular pattern of air circulation is shown by rational responses of carbon dioxide pressure to visitor periods. The following calculations apply to these periods. Where the rise is clear and visitor numbers are known, the rise in CO<sub>2</sub> in relation to the number of adult visitor-hours allows a calculation of cave volume (5800 m<sup>3</sup>), which is broadly consistent with its geometric volume. A distinct exponential decay in pCO<sub>2</sub> was also found in these cases during the evening. This allows the air-exchange time with the exterior to be calculated as 1.8 to 6 hours, with the median being 3.5 hours. Some of the fastest times were found in July and August and hence the rate of air-exchange is not in this case, unlike many others, responsible for seasonal changes in pCO<sub>2</sub>. A simple mass-balance model allows the fluxes of CO<sub>2</sub> in and out of the cave in kg day<sup>-1</sup> to be estimated as 25 – 50 and 160 – 330 in summer and 25 – 50 and 28 – 56 in winter, respectively. The difference represents the net CO<sub>2</sub> production in the cave (release from stream and drip water, input from epikarst fissures, oxidation of organic matter, minus dissolution in hyperalkaline water). The amounts in winter are similar to those produced by visitors in a busy day (3.5 to 6.5, equivalent to 110 – 220 visitor-hours), whereas in summer, the net production is 50 times higher and is not influenced significantly by visitors. The difference might be attributed to some combination of a seasonal change in stream water composition and the winter filling of air fissures in epikarst by water.

Examination of the petrology of the stalagmite samples reveals a previously undescribed fabric in which columnar crystals nucleate along arcs, spaced at sub-mm-scale intervals that are commonly more convex than the pale-dark annual growth bands. They therefore cross time lines and appear to accrete sideways. A radiocarbon study was carried out to establish whether the cave air is indeed the primary source of C in the stalagmite. The 20<sup>th</sup> century peak in <sup>14</sup>C, caused

by atmospheric nuclear testing, is well-displayed in the data, with a maximum value of 140 absolute % modern carbon in 1965, close in timing to the peak in the external atmosphere. In 1950, the sample had 84% modern carbon and hence a dead-carbon percentage (from limestone) of 16%. Cave air is close in radiocarbon activity to that of the external atmosphere but, as expected the  $\delta^{13}\text{C}$  signature becomes more negative as  $p\text{CO}_2$  increases, because the external air has a value of around -8‰ and anthropogenic and other  $\text{CO}_2$  sources are expected to be around -25 to -27‰. A pronounced annual variability in  $\delta^{13}\text{C}$  and  $\delta^{18}\text{O}$  in the speleothem is found, with the former displaying a range of -35 to -44‰ and the latter -21 to -23‰. These values are consistent with the experiments and theoretical arguments of Clark *et al.* (1992), who showed that the key controls were the composition of the source  $\text{CO}_2$  and the presence of strong fractionation of  $^{13}\text{C}$  during the essentially irreversible  $\text{CO}_2$  hydroxylation reaction ( $\text{CO}_2 + \text{OH}^- \rightarrow \text{HCO}_3^-$ ) coupled with the strong isotope depletion of  $^{18}\text{O}$  in the reactant  $\text{OH}^-$ .

## Summary

We have shown that high pH conditions in Poole's Cavern hyperalkaline dripwaters result in both higher concentrations of colloidal organic matter and apparently, greater reactivity of organic ligands, reflected in stronger binding of transition metal ions ( $\text{Cu}, \text{Ni} > \text{Co}$ ). Natural colloidal entities exist in a continuum from the particulate to the nanoparticulate. Although their stability in solution is thought to be enhanced under high pH conditions, we found no compositional or morphological difference between colloidal aggregates in normal (alkaline) and hyperalkaline dripwaters. Hence, information relating to their trace element binding behaviour should be relevant to cave dripwaters in general. Based on their elemental composition, colloids were considered to be largely composed of organic matter in association with aluminosilicates and iron oxides and some evidence for the association of Ti and Mn in colloidal aggregates was found.

In order to complete our understanding of the Poole's Cavern system, we need to determine the variation in growth rate within the year and the isotope characteristics of the source  $\text{CO}_2$  and this includes an examination of their clumped isotope characteristics, i.e. the extent to which doubly-substituted heavy isotopes ( $^{13}\text{C}^{18}\text{O}^{16}\text{O}_2$ ) preferentially occur (Eiler, 2007). A high-pH system allows a test of theoretical insights (Guo *et al.*, in prep.). Our ongoing work on the trace element composition of the stalagmites will also provide insights into how organic species carrying trace elements interact with calcite surfaces. Hence Poole's Cavern's hyperalkaline environment, its dripwaters and its stalagmites, provide a superb model chemical system for developing understanding of environmental processes.

## Acknowledgements

Staff of Poole's Cavern and Buxton Civic Association are thanked for their help in facilitating this research. The work was partially funded through an award to AH through the BCRA Cave Science and Technology Research Initiative, and AH was also supported by a NERC studentship (NER/S/A/2007/14396). The authors gratefully acknowledge the support of the NERC Facility for Environmental Nanoscience Analysis and Characterisation. Thanks also to Kevin Burkhill for redrawing cave schematics from original drawings by P R Deakin and members of the Eldon Pothole Club (February 1968). Thanks to the Environment Agency (UK) Geomatics Group for provision of LIDAR data under licence.

## References

Baker, A. 2001. Fluorescence Excitation-Emission Matrix Characterization of Some Sewage-Impacted Rivers. *Environmental Science and Technology*, Vol.35, 948–953.

Baker, A, Genty D, Dreybrodt W, Barnes W L, Mockler N J, Grapes J. 1998. Testing theoretically predicted stalagmite growth rate with Recent annually laminated samples: Implications for past stalagmite deposition. *Geochimica et Cosmochimica Acta*, Vol.62, 2405–2405.

Baker, A and Genty, D. 1999. Fluorescence wavelength and intensity variations of cave waters. *Journal of Hydrology*, Vol.217, 19–34.

Baker, A, Proctor, C J and Barnes, W L. 1999. Variations in stalagmite luminescence laminae structure at Poole's Cavern, England, AD 1910-1996: calibration of a palaeoprecipitation proxy. *Holocene*, Vol.9, 683–688.

Baker, A, Tipping, E, Thacker, S A and Gondar, D. 2008. Relating dissolved organic matter fluorescence and functional properties. *Chemosphere*, Vol.73, 1765–1772.

Borsato, A, Frisia, S, Fairchild, IJ, Somogyi, A and Susini, J. 2007. Trace element distribution in annual stalagmite laminae mapped by micrometer-resolution X-ray fluorescence: Implications for incorporation of environmentally significant species. *Geochimica et Cosmochimica Acta*, Vol.71, 1494–1512.

Bradl, H B. 2004. Adsorption of heavy metal ions on soils and soils constituents. *Journal of Colloid and Interface Science*, Vol.277, 1–18.

Buffle, J, Wilkinson, K J, Stoll, S, Filella, M and Zhang, J W. 1998. A generalized description of aquatic colloidal interactions: The three-colloidal component approach. *Environmental Science and Technology*, Vol.32, 2887–2899.

Chen, C-C and Hayes, K F. 1999. X-ray absorption spectroscopy investigation of aqueous  $\text{Co}(\text{II})$  and  $\text{Sr}(\text{II})$  sorption at clay-water interfaces. *Geochimica et Cosmochimica Acta*, Vol.63, 3205–3215.

Clark, I D, Fontes, J-C and Fritz, P. 1992. Stable isotope disequilibria in travertine from high pH waters: laboratory investigations and field observations from Oman. *Geochimica et Cosmochimica Acta*, Vol.56, 2041–2050.

Eiler, J M. 2007. "Clumped-isotope" geochemistry – the study of naturally-occurring, multiply-substituted isotopologues. *Earth and Planetary Science Letters*, Vol.262, 309–327.

Faimon, J, Štelcl, J and Sas, D. 2006. Anthropogenic  $\text{CO}_2$ -flux into cave atmosphere and its environmental impact: A case study in the Císarská Cave (Moravian Karst, Czech Republic). *Science of the Total Environment*, Vol.369, 231–245.

Fairchild, I J and Hartland, A. 2010. Trace element variations in stalagmites: controls by climate and by karst system processes. In Stoll, H and Prieto, M (editors), Ion partitioning in ambient temperature aqueous systems: from fundamentals to applications in climate proxies and environmental geochemistry, Vol.8, European Mineralogical Union, Oviedo.

Ford, T D and Gunn, J. 1992. Caves and Karst of the Peak District. *BCRA Cave Studies*, Vol.3.

Gill, D W and Beck, J S. 1991. *Caves of the Peak District*. [Lancaster: Dalesman.]

Guo, W, Daëron, M, Niles, P B, Goddard, W A, Eiler, J M. [in prep.] Isotopic fractionations associated with degassing of  $\text{CO}_2$  from aqueous solutions: implications for carbonate clumped isotope thermometry. *Geochimica et Cosmochimica Acta*.

Hartland, A, Fairchild, I J, Lead, J R and Baker, A. [in prep.] Fluorescent properties of organic carbon in cave dripwaters: effects of filtration, temperature and pH. *Science of the Total Environment*.

Lakowicz, J R. 2006. *Principles of Fluorescence Spectroscopy*. 3<sup>rd</sup> Edition. [Springer.] 954 pp.

Lead, J R and Wilkinson, K J. 2006. Aquatic colloids and nanoparticles: Current knowledge and future trends. *Environmental Chemistry*, Vol.3, 159–171.

Macleod, G, Fallick, A E and Hall, A J. 1991. The mechanism of carbonate growth on concrete structures, as elucidated by carbon and oxygen isotope analyses. *Chemical Geology*, Vol.86, 335–343.

Mavrocordatos, D, Mondy-Couture, C, Atteia, O, Leppard, G G and Perret, D. 2000. Formation of a distinct class of Fe-Ca-(C-org)-rich particles in a complex peat-karst system. *Journal of Hydrology*, Vol.237, 234–247.

McDermott, F, Frisia, S, Huang, Y M, Longinelli, A, Spiro, B, Heaton, T H E, Hawkesworth, C J, Borsato, A, Keppens, E, Fairchild, I J, van der Borg, K, Verheyden, S and Selmo, E. 1999. Holocene climate variability in Europe: Evidence from delta O-18, textural and extension-rate variations in three speleothems. *Quaternary Science Reviews*, Vol.18, 1021–1038.

Mobed, J J, Hemmingsen, S L, Autry, J L and McGown, L B. 1996. Fluorescence characterization of IHSS humic substances: Total luminescence spectra with absorbance correction. *Environmental Science and Technology*, Vol.30, 3061–3065.

Patel-Sorrentino, N, Mounier, S and Benaïm, J Y. 2002. Excitation-emission fluorescence matrix to study pH influence on organic matter fluorescence in the Amazon basin rivers. *Water Research*, Vol.36, 2571–2581.

Pitty, A F. 1966. An approach to the study of karst water. *University of Hull Occasional Papers in Geography*, Vol.5, 210–230.

Richter, D K, Gotte, T, Niggemann, S and Wurth, G. 2004.  $\text{REE}^{3+}$  and  $\text{Mn}^{2+}$  activated cathodoluminescence in lateglacial and Holocene stalagmites of central Europe: evidence for climatic processes? *Holocene*, Vol.14, 759–767.

Smithson, P. 1991. Inter-relationships between cave and outside air temperatures. *Theoretical and Applied Climatology*, Vol.44, 65-73.

Spencer, R G M, Bolton, L and Baker, A. 2007. Freeze/thaw and pH effects on freshwater dissolved organic matter fluorescence and absorbance properties from a number of UK locations. *Water Research*, Vol.41, 2941–2950.

Sundqvist, H S, Baker, A and Holmgren, K. 2005. Luminescence variations in fast-growing stalagmites from Uppsala, Sweden. *Geografiska Annaler Series A - Physical Geography*, Vol.87A, 539–548.

Tam, S C and Sposito, G. 1993. Fluorescence spectroscopy of aqueous pine litter extracts - effects of humification and aluminium complexation. *Journal of Soil Science*, Vol.44, 513–524.

Tipping, E. 2001. *Cation binding by humic substances*. [Cambridge: University Press.]

Wilkinson, K J, Balnois, E, Leppard, G G and Buffle, J. 1999. Characteristic features of the major components of freshwater colloidal organic matter revealed by transmission electron and atomic force microscopy. *Colloids and Surfaces A: Physicochemical and Engineering Aspects*, Vol.155, 287–310.

Zhang, P-C, Brady, P V, Arthur, S E, Zhou, W-Q, Sawyer, D and Hesterberg, D A. 2001. Adsorption of barium(II) on montmorillonite: an EXAFS study. *Colloids and Surfaces A: Physicochemical and Engineering Aspects*, Vol.190, 239–249.